

A universal 21 cm signature of growing massive black holes in the early Universe

S. Sazonov^{1,2*} and I. Khabibullin^{3,1}

¹*Space Research Institute, Russian Academy of Sciences, Profsoyuznaya 84/32, 117997 Moscow, Russia*

²*Moscow Institute of Physics and Technology, Institutskiy per. 9, 141700 Dolgoprudny, Russia*

³*Max Planck Institute for Astrophysics, Karl-Schwarzschild-Strasse 1, D-85741 Garching, Germany*

21 June 2022

ABSTRACT

There is a hope that looking into the early Universe with next-generation telescopes, one will be able to observe the early accretion growth of supermassive black holes (BHs) when their masses were $\sim 10^4\text{--}10^6 M_\odot$. According to the standard theory, the bulk of the gravitational potential energy released during radiatively efficient accretion onto a BH in this mass range is expected to fall into the extreme UV–ultrasoft X-ray band. We demonstrate that such a ‘miniquasar’ at $z \sim 15$ should leave a specific, localized imprint on the 21 cm cosmological signal. Namely, its position on the sky will be surrounded by a region with a fairly sharp boundary of several arcmin radius, within which the 21 cm brightness temperature quickly grows inwards from the background value of ~ -200 mK to $\sim +30$ mK. The size of this region is only weakly sensitive to the BH mass, so that the flux density of the excess 21 cm signal is expected to take a nearly universal value of $\sim 0.2[(1+z)/16]^{-2}$ mJy and should be detectable by the Square Kilometer Array. We argue that an optimal strategy would be to search for such signals from high- z miniquasar candidates that can be found and localized with a next-generation X-ray mission such as *Lynx*. A detection of the predicted 21 cm signal would provide a measurement of the growing BH’s redshift to within $\Delta z/(1+z) \lesssim 0.01$.

Key words: stars: black holes – accretion, accretion discs – galaxies: high-redshift – dark ages, reionization, first stars – quasars: supermassive black holes

1 INTRODUCTION

The discovery of powerful quasars at $z \approx 7.5$ (Bañados et al. 2018) implies that fully fledged supermassive black holes (BHs), as heavy as $M_{\text{BH}} \sim 10^9 M_\odot$, already existed when the Universe was just 700 million years old. If a significant fraction of this mass has been accumulated by accretion at a nearly critical rate (rather than by BH mergers), then the growth of such objects must have started very early on (at $z \gtrsim 20$) from seeds that already had masses $\sim 10^3 M_\odot$ or more. What kind of object these seeds were is one of the most interesting open questions in astrophysics (see Volonteri 2010; Latif & Ferrara 2016; Woods et al. 2018 for reviews). There is a hope that looking into the $z \sim 20\text{--}10$ epochs with next-generation telescopes, one will be able to observe the early accretion growth of supermassive BHs when their masses were $\sim 10^4\text{--}10^6 M_\odot$. Hereafter, we will refer to such accretors as ‘miniquasars’.

One of the most promising ways to find such mini-

quasars is in X-rays, since we know that both stellar-mass and supermassive black holes emit copious amounts of X-rays during accretion (X-ray binaries, XRBs, and active galactic nuclei, AGN, respectively). Unfortunately, even the sensitivity of the *Chandra X-ray Observatory* is not sufficient to detect miniquasars at $z \gtrsim 6$. The situation will change dramatically if a mission such as the proposed *Lynx* is implemented in the future. *Lynx* is planned to achieve a sensitivity as high as 10^{-19} erg cm⁻² s⁻¹ (0.5–2 keV), in combination with *Chandra*-like (arcsecond) angular resolution and substantial sky coverage (~ 1 sq. deg), in its deep extragalactic surveys (Ben-Ami, Vikhlinin, & Loeb 2018). This implies that X-sources with luminosities as low as a few 10^{41} erg s⁻¹ (rest-frame 2–10 keV) will be detectable without confusion at $z \sim 15$. Assuming that hard X-ray emission carries a significant ($\sim 10\%$) fraction of the near-Eddington bolometric luminosity of a miniquasar, *Lynx* will be able to detect accreting BHs with masses as low as a few $10^4 M_\odot$ in the early Universe.

The bulk of the gravitational potential energy released during radiatively efficient accretion onto a BH emerges in

* E-mail: sazonov@iki.rssi.ru

the form of quasi-thermal radiation from the accretion disk (Shakura & Sunyaev 1973), with the effective waveband shifting from the optical–UV for supermassive BHs to soft X-rays for stellar-mass BHs, as observed in AGN and XRBs (in so-called soft/high states for the latter, e.g. Gilfanov & Merloni 2014). For intermediate-mass BHs, the bulk of the disk’s emission is expected to fall into the far UV–ultrasoft X-ray band. Therefore, due to cosmological redshift, *Lynx* will not be able to detect this primary emission component, but, as already mentioned above, it should be able to observe additional, harder radiation that can arise due to Comptonization of thermal emission from the disk in its hot corona. In principle, the redshifted thermal disk emission from miniquasars could be observed directly in the optical–infrared band, but its detection will be extremely challenging even with the next-generation telescopes such as the *James Web Space Telescope*¹ and the Extremely Large Telescope², since the Eddington luminosity for a BH of mass $\sim 10^5 M_\odot$ at $z \sim 15$ corresponds to an AB magnitude of more than 30, the anticipated limiting magnitude of these telescopes.

There is, however, another, indirect way to reveal the thermal disk emission from the first miniquasars, which is to observe its impact on the ambient intergalactic medium (IGM) in the early Universe using the 21 cm spin-flip transition of neutral hydrogen. As has been actively discussed over the past two decades, the first generations of X-ray sources could significantly heat the primordial IGM prior to cosmic reionization and strongly modify the global 21 cm signal from the $z \sim 15$ – 10 epochs (see Pritchard & Loeb 2012 for a review). A lot of recent literature on this subject is devoted to discussing the potentially observable effect of the first generations of stellar-type X-ray sources and in particular high-mass X-ray binaries (HMXBs, e.g. Mirabel et al. 2011; Cohen et al. 2017; Madau & Fragos 2017; Sazonov & Khabibullin 2017), which should have been present in significant numbers since the beginning of active star formation in the Universe (Fragos et al. 2013). The bulk of the emission produced by HMXBs is at energies above 0.5 keV and since such photons can travel large distances before being photoabsorbed in the IGM, the main effect of HMXBs is expected to be a global enhancement of the IGM temperature together with large-scale fluctuations reflecting the large-scale structure in the early Universe (e.g. Pritchard & Furlanetto 2007; Ross et al. 2017).

In contrast, miniquasars, which presumably have much softer energy spectra compared to HMXBs, should mainly heat the IGM in their relatively close vicinity. One may thus expect such sources to be surrounded by compact regions of specific 21 cm signal. Although finding such 21 cm features in a blind search would be difficult even for the most ambitious upcoming radio telescopes such as the Square Kilometer Array (SKA, Mellema et al. 2013), such a search could be greatly facilitated if carried out around miniquasar candidates found via their coronal X-ray emission with a mission like *Lynx*. We elaborate on this idea in the present paper. Before proceeding, we note that there have been plenty of studies addressing the impact of quasars and miniquasars on the IGM and the associated 21 cm signal (e.g. Madau et al.

2004; Ricotti & Ostriker 2004; Chuzhoy, Alvarez, & Shapiro 2006; Thomas & Zaroubi 2008; Fialkov et al. 2017; Ghara et al. 2017; Bolgar et al. 2018; Vasiliev, Sethi, & Shchekinov 2018), but the novelty of our study is its focus on the miniquasar primary, thermal emission component and the synergy of 21 cm and X-ray observations.

The following values of cosmological parameters are used below: $\Omega_m = 0.309$, $\Omega_\Lambda = 1 - \Omega_m$, $\Omega_b = 0.049$, $H_0 = 68 \text{ km s}^{-1} \text{ Mpc}^{-1}$ and $Y = 0.246$ (helium mass fraction).

2 MODEL

Suppose a BH has an initial mass M_i at redshift z_i and accretes matter until epoch z_f , reaching a final mass M_f . If the accretion proceeded at a critical (Eddington limited) rate \dot{M}_E , the BH mass would be increasing exponentially,

$$M(t) = M_i e^{\frac{t}{t_S}}, \quad (1)$$

on the Salpeter time scale $t_S = \frac{\epsilon}{1-\epsilon} \frac{c^2 M_\odot}{L_{\text{Edd}}(M_\odot)}$, where L_{Edd} is the Eddington luminosity and ϵ is the radiation efficiency. Adopting for simplicity $\epsilon = 0.1$ (as is approximately true for standard accretion disks), $t_S \approx 5 \times 10^7 \text{ yr}$. Therefore, the average rate expressed in units of the critical rate (usually referred to as the Eddington ratio), at which the BH accretes mass between epochs z_i and z_f is

$$\langle \dot{m} \rangle \equiv \frac{\dot{M}}{\dot{M}_E} = \frac{t_S}{t(z_i, z_f)} \ln \frac{M_f}{M_i}, \quad (2)$$

where $t(z_i, z_f)$ is the cosmic time between z_i and z_f .

It is unlikely though that the BH will accrete matter at a constant rate over a cosmologically long period of time. In reality, accretion of gas onto the BH will be determined by evolving external and internal (with respect to the host galaxy) conditions and is likely to be an intermittent process. Therefore, in our simulations described below, we assumed that there are periods of active accretion, when the Eddington ratio takes a fixed value \dot{m} , and passive periods when $\dot{m} = 0$. We further assume that these two types of intervals alternate in a random fashion³, so that the duty cycle of BH activity is

$$k_{\text{duty}} = \frac{\langle \dot{m} \rangle}{\dot{m}}. \quad (3)$$

By definition, $\dot{m} \geq \langle \dot{m} \rangle$, and we also assume that $\dot{m} < 1$, i.e. we do not consider supercritical accretion in this study.

2.1 Emission spectrum

One of the key aspects for this study is the spectrum of the radiation emitted by the accreting BH. According to the standard theory (Shakura & Sunyaev 1973), a geometrically thin, optically thick accretion disk around a BH is characterized by a $\propto r^{-3/4}$ temperature profile (except in the very narrow innermost region, where only a small fraction of the total luminosity is emitted) and generates multicolor, nearly

¹ <https://jwst.nasa.gov/>

² <https://www.eso.org/sci/facilities/eelt/>

³ We took the duration of these intervals $\Delta t = 10^4$ or 10^5 yr , with the results being insensitive to this choice as long as $\Delta t \ll t_S$.

blackbody radiation with a spectrum (specific luminosity as a function of energy)

$$L_E(E) \propto \int_{r_{\text{in}}}^{r_{\text{out}}} r B_E(E, T(r)) dr, \quad (4)$$

where r_{in} and r_{out} are the disk's inner and outer radii and B_E is the Planck function.

The maximum temperature of the disk is

$$kT_{\text{max}} \approx 1.2 \left(\frac{\dot{m}}{m} \right)^{1/4} \text{ keV}, \quad (5)$$

where $m(t)$ is the BH mass expressed in solar masses, which grows with time. According to the standard theory, this temperature is achieved at $(49/36)r_0$, where r_0 is the radius of the innermost stable circular orbit, but a fairly good approximation is to assume that the disk temperature reaches this value at r_{in} and then decreases as $T(r) = T_{\text{max}}(r/r_{\text{in}})^{3/4}$ at $r > r_{\text{in}}$. For the purposes of this study, it can also be safely assumed that $r_{\text{out}} \rightarrow \infty$. The spectrum given by equation (4) can then be approximated by a power law, $L_E \propto E^{1/3}$ at $E \lesssim 0.3kT_{\text{max}}$ and by a single blackbody spectrum with a temperature $0.7T_{\text{max}}$ at $E \gtrsim 2kT_{\text{max}}$ (Makishima et al. 1986), with its maximum (when plotted in units of EL_E) being at $E_{\text{max}} \approx 2.35kT_{\text{max}}$. The normalization constant in equation (4) is determined by the condition

$$\int L_E dE = \dot{m} L_{\text{Edd}}(m). \quad (6)$$

The model described above is widely known as a multicolor disk blackbody model (*diskbb* in XSPEC, Arnaud 1996), and it is this simplistic model that we have chosen as our baseline spectral model. This choice is primarily motivated by the fact that the standard accretion disk theory provides a satisfactory description of the observed spectral energy distributions (SED) of (i) XRBs in their soft/high states (when $\dot{m} \gtrsim 0.1$); namely, their dominant emission component is well described by *diskbb* with $kT_{\text{max}} \lesssim 1$ keV, as expected from equation (5) for the stellar masses ($m \lesssim 10$) of the BHs in XRBs (see Done, Gierliński, & Kubota 2007 for a review) and (ii) AGN – supermassive BHs accreting at $\dot{m} \sim 0.01$ –1, for which the peak of the SED is observed in the optical-UV (the so-called big blue bump, e.g. Elvis et al. 1994; Telfer et al. 2002; Sazonov, Ostriker, & Sunyaev 2004), again as expected from equation (5) for the high ($m \sim 10^7$ – 10^9) BH masses of AGN.

In reality, observations reveal significant deviations of XRB and AGN spectra from the simple multicolor disk blackbody model described above, and these deviations can be generally accounted for by the conditions at the inner boundary of the accretion disk, radiative transfer effects in the disk's atmosphere and relativistic corrections (e.g. Koratkar & Blaes 1999; Merloni, Fabian, & Ross 2000; Davis et al. 2005; Done et al. 2012). However, in view of other, larger uncertainties related to the problem at hand (in particular in the BH mass and accretion rate), we do not take these subtleties into account.

Arguing further from analogy with XRBs and AGNs, it is likely that a miniquasar's emission spectrum has an additional, harder component, due to Comptonization of a fraction of the thermal radiation of the disk in a hot corona. We simulate this plausible situation by modifying our baseline *diskbb* model by the *simpl* (Steiner et al. 2009) model [specifically we use *simpl(diskbb)* in XSPEC], which provides a sim-

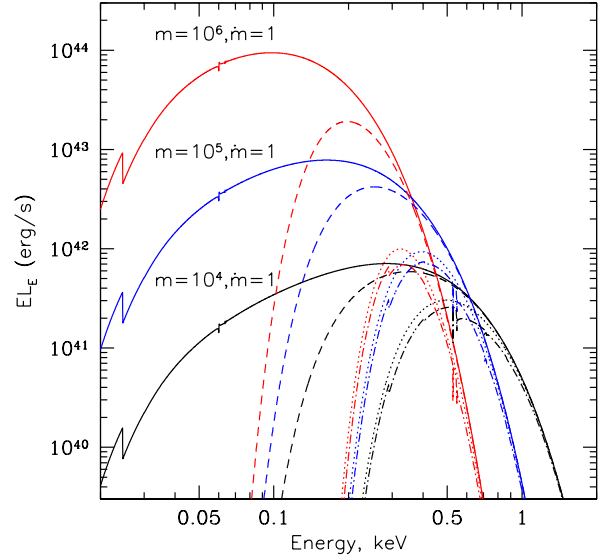


Figure 1. Multicolor disk blackbody emission spectra (in the source's rest frame, in units of its specific luminosity multiplied by photon energy) modified by absorption in the miniquasar's host galaxy, for $\dot{m} = 1$, different BH masses, $m = 10^4$ (black), 10^5 (blue) and 10^6 (red), and various absorption columns and metallicities (N_{H} in cm^{-2} , Z): $(10^{18}, 0)$ – solid, $(10^{20}, 0)$ – dashed, $(10^{21}, 0)$ – dotted, $(10^{21}, 1)$ – dash-dotted.

plified description of Comptonization by converting a given fraction, f_{sc} , of soft thermal photons into high-energy ones. Another free parameter of this model is the photon index, Γ , of the powerlaw component. We use $\Gamma = 2$ and $f_{\text{sc}} = 0.05$ as fiducial values. The assumed spectral slope is close to those of hard X-ray tails in XRBs and AGN and is convenient in use since no k -correction is then needed in converting luminosities to fluxes. The adopted f_{sc} value implies that the powerlaw component, if it continues up to $E \sim 100$ keV, contains $\sim 25\%$ (with a very weak dependence on the disk temperature, i.e. on m and \dot{m}) of the miniquasar's bolometric luminosity, in overall agreement with observations of XRBs in their high state (e.g. Done, Gierliński, & Kubota 2007) and AGN (e.g. Sazonov, Ostriker, & Sunyaev 2004).

We finally note that, as was already mentioned above, our current consideration is restricted to the case of subcritical accretion ($\dot{m} < 1$). In reality, it cannot be excluded that in some miniquasars and/or at some stage of their evolution, accretion proceeds at a supercritical rate. In order to consider such a case, it would be necessary to adopt a substantially different spectral model, as, in particular, suggested by the specific SEDs of ultraluminous X-ray sources in nearby galaxies (e.g. Sazonov, Lutovinov, & Krivonos 2014).

2.2 Intragalactic absorption

Before reaching the ambient IGM, the extreme UV-soft X-ray radiation from the miniquasar may be partially photoabsorbed within its host galaxy. This may happen (i) in the vicinity of the BH, if something like the AGN obscur-

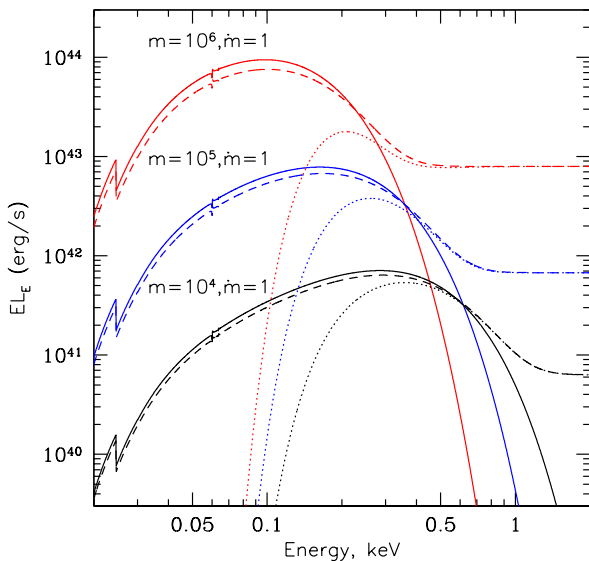


Figure 2. Multicolor disk blackbody emission spectra modified by Comptonization (*simpl(diskbb)*), for the same BH masses as in Fig. 1 (shown with the same colors). The dashed and dotted curves correspond to $N_{\text{H}} = 10^{18} \text{ cm}^{-2}$ and $N_{\text{H}} = 10^{20} \text{ cm}^{-2}$, respectively ($Z = 0$). The solid curves show the pure thermal spectra.

ing torus is present in miniquasars (in that case, absorption will take place within a certain solid angle only), and/or (ii) in the more distant regions of the galaxy. Given our scarce knowledge about the first galaxies and in particular about the parsec-scale environment of intermediate-mass BHs they may host, and also taking into account that the miniquasar’s radiation can significantly ionize the interstellar medium in front of it and thereby strongly diminish the net absorption effect (see, e.g., Sazonov & Khabibullin 2018), it is hardly possible to provide a robust prediction for the line-of-sight absorption columns, N_{H} , pertaining to miniquasars in the early Universe. We therefore consider it a free parameter. Similarly, we allow the metallicity of the absorbing gas to vary from $Z = 0$ (pure H–He gas) to $Z = 1$ (normal chemical composition). The reason for this is that although the first galaxies (at $z \sim 20\text{--}10$) were likely metal poor, the immediate surroundings of miniquasars might have been significantly metal enriched because they were probably the sites of particularly strong star formation activity.

Figure 1 shows examples of (rest-frame) spectra of miniquasars for various values of model parameters, namely m (assuming $\dot{m} = 1$), N_{H} and Z (absorption was modeled by means of the *tbvarabs* model in XSPEC). We see that for the range of BH masses and accretion rates expected for miniquasars and in the absence of absorption, the bulk of the emission is in the extreme UV–very soft X-ray band, at energies $E \sim 50\text{--}1000 \text{ eV}$. Even a moderate absorption ($N_{\text{H}} \lesssim 10^{20} \text{ cm}^{-2}$) causes a strong reduction of the flux below $\sim 200 \text{ eV}$. An addition of metals to the absorbing medium (the $Z = 1$ case) additionally reduces the flux, but mostly above the oxygen absorption edge at $E = 536 \text{ eV}$.

Figure 2 shows examples of thermal disk spectra modi-

fied by Comptonization, as described above. For the adopted value, $f_{\text{sc}} = 0.05$, of the fraction of Comptonized photons, the hard tail starts to dominate over the disk emission at $\sim 1 \text{ keV}$ for the lowest mass BH ($m = 10^4$) and already at $\sim 300 \text{ eV}$ for the highest mass BH ($m = 10^6$).

3 A CRUDE ESTIMATE OF THE EXPECTED HEATING

To a first approximation, the thermal disk emission from miniquasars (with $m \sim 10^4\text{--}10^6$) in the presence of moderate absorption ($N_{\text{H}} \lesssim 10^{20} \text{ cm}^{-2}$) may be characterized by a narrow spectrum around an energy $E = 300 \text{ eV}$ (see Fig. 1). This allows us to derive order-of-magnitude estimates for the impact of a miniquasar on the IGM before proceeding to detailed numerical calculations.

The mean free path of soft X-ray photons of energy E in the primordial (i.e. nearly neutral H–He gas) IGM of the early Universe can be approximated as follows (Sazonov & Sunyaev 2015):

$$\bar{\lambda} \approx 740 \left(\frac{1+z}{11} \right)^{-3} \left(\frac{E}{300 \text{ eV}} \right)^{3.2} \text{ kpc}. \quad (7)$$

Within this (proper) distance from the source, $1 - e^{-1} \approx 63\%$ of photons of energy E will be photoabsorbed (whereas 95% of photons will be absorbed within $3\bar{\lambda}$). The distance $\bar{\lambda}$ corresponds to an angular size

$$\bar{\theta} \approx 2.7 \left(\frac{1+z}{11} \right)^{-2} \left(\frac{E}{300 \text{ eV}} \right)^{3.2} \text{ arcmin}, \quad (8)$$

on the sky, which is a reasonably good approximation for $z = 20\text{--}10$ and $E = 100\text{--}1000 \text{ eV}$.

The thermal disk emission from a miniquasar can heat the IGM efficiently only within a few $\bar{\lambda}$, since only an exponentially decreasing fraction of the miniquasar’s luminosity reaches larger distances. This allows us to readily estimate the expected IGM temperature increment. The total energy released by the BH during its growth to mass M is $W = \epsilon M c^2$ and we may assume that most of this energy is radiated away over a time of order the Salpeter time (t_{S}) just before the epoch when the miniquasar and the associated 21 cm signal are actually observed, so that, to a first approximation, we can ignore any effects associated with the expansion of the Universe. We may further assume that all of this energy has been absorbed within a volume of radius $\sim \bar{\lambda}$ (the corresponding light travel time proves to be shorter than t_{S}). Assuming that the miniquasar ionizes the surrounding medium only moderately (i.e. the ionization degree of hydrogen is less than a few per cent, which is a good approximation for the bulk of the affected volume), we may roughly estimate the mean fraction of the energy of soft X-ray photons that goes into heating the IGM as $f_{\text{heat}} \sim 0.2$ (Furlanetto & Stoever 2010). Taking into account that the hydrogen space density changes with redshift as $n_{\text{H}}(z) \approx 2.6 \times 10^{-4} [(1+z)/11]^3 \text{ cm}^{-3}$, we can write

$$f_{\text{heat}} W = \frac{4\pi\bar{\lambda}^3}{3} \frac{3}{2} n_{\text{H}} k \Delta T_{\text{K}}, \quad (9)$$

where k is the Boltzmann constant, and finally determine the

expected IGM temperature increment assuming $E = 300$ eV:

$$\Delta T_K \sim 100 \frac{f_{\text{heat}}}{0.2} \frac{\epsilon}{0.1} \left(\frac{1+z}{11} \right)^6 \frac{m}{10^4} \text{ K}. \quad (10)$$

Comparing this with the cosmic microwave background (CMB) temperature, $T_{\text{CMB}}(z) \approx 30[(1+z)/11]$, we come to the conclusion that BHs with $M \gtrsim 10^4 M_\odot$ accreting at a nearly critical rate in the early Universe are expected to be surrounded by well-defined zones with a radius of a few arcmin within which $T_K \gtrsim T_{\text{CMB}}$, and these regions are thus expected to be 21 cm emitters, in contrast to the surrounding sky, which is likely to exhibit 21 cm absorption at $z \gtrsim 10$. Importantly, for $m \gtrsim 10^4$, the size of the heating region is determined simply by the mean free path of soft X-ray photons, rather than by the radiative power of the miniquasar. Following the same argument, we may expect that for BHs of smaller mass, $m \lesssim 10^4$, the region of strong heating ($\Delta T_K \gtrsim T_{\text{CMB}}(z)$) will be smaller than $\sim \bar{\lambda}$, i.e. the heating zone will be limited by the total accretion energy released by accretion onto the BH.

4 SIMULATIONS

Based on the assumptions outlined in §2, we performed a series of numerical calculations of IGM heating and associated 21 cm emission/absorption in the vicinity of miniquasars in the early Universe. We limited computations to a redshift range of $z = 20$ – 10 and neglected any global heating (i.e. outside the region affected by the miniquasar) of the IGM by X-ray sources and/or other mechanisms⁴. Therefore, we adopted the following initial parameters of the IGM: $x_{\text{HII}} \equiv n_{\text{HII}}/n_{\text{H}} = 2.2 \times 10^{-4}$ (hydrogen ionization fraction), $x_{\text{HeII}} \equiv n_{\text{HeII}}/n_{\text{He}} = 0$, $x_{\text{HeIII}} \equiv n_{\text{HeIII}}/n_{\text{He}} = 0$ (helium ionization fractions) and $T_K = 9.3$ K (for $z_i = 20$) or $T_K = 5.4$ K (for $z_i = 15$). These were found using RECFAST (Seager, Saselov, & Scott 1999) and correspond to the conditions after cosmic recombination and adiabatic cooling of the primordial gas. Our assumption about the absence of significant global heating might be a good approximation at least at $z \gtrsim 15$, as suggested by the recent detection of a strong, sky-averaged 21 cm absorption signal in the Experiment to Detect the Global Epoch of Reionization Signature (EDGES, Bowman et al. 2018).

X-ray ionization and heating of the IGM was calculated in logarithmically binned spherical shells around the miniquasar, out to a comoving distance of 500 Mpc. Although this maximal distance is fairly large, we ignored photon travel time effects (i.e. the response of the IGM to radiation emitted by the central source was considered instantaneous), since X-ray heating proves to be noticeable only within ~ 30 cMpc of the miniquasar, so that the corresponding light travel time at $z \gtrsim 10$ is much shorter than the Salpeter timescale on which BH growth occurs.

The evolution of the ionization state of hydrogen and helium with time in a given shell was calculated as follows:

$$\frac{dx_{\text{HI}}}{dt} = -x_{\text{HI}}\Gamma_{\text{HI}} + n_e(1 - x_{\text{HI}})\alpha_{\text{HII}},$$

⁴ In particular, by low-energy cosmic rays from the first supernovae (Sazonov & Sunyaev 2015; Leite et al. 2017).

$$\begin{aligned} \frac{dx_{\text{HeI}}}{dt} &= -x_{\text{HeI}}\Gamma_{\text{HeI}} + n_e x_{\text{HeII}}\alpha_{\text{HeIII}}, \\ \frac{dx_{\text{HeII}}}{dt} &= -x_{\text{HeII}}\Gamma_{\text{HeII}} + n_e x_{\text{HeIII}}\alpha_{\text{HeIII}} - \frac{dx_{\text{HeI}}}{dt}, \end{aligned} \quad (11)$$

where n_e is the number density of free electrons, α_{HII} , α_{HeII} and α_{HeIII} are the recombination coefficients (adopted from Theuns et al. 1998), and Γ_{HI} , Γ_{HeI} and Γ_{HeII} are the photoionization coefficients, which were calculated as follows:

$$\begin{aligned} \Gamma_{\text{HI}} &= \frac{1}{4\pi r^2} \left(\int_{I_{\text{HI}}}^{\infty} \frac{L_E e^{-\tau(r,E)}}{E} \sigma_{\text{HI}} (1 + N_{\text{s,HI}}(E - I_{\text{HI}})) dE \right. \\ &\quad + \int_{I_{\text{HeI}}}^{\infty} \frac{L_E e^{-\tau(r,E)}}{E} \sigma_{\text{HeI}} \frac{n_{\text{HeI}}}{n_{\text{HI}}} N_{\text{s,HI}}(E - I_{\text{HeI}}) dE \\ &\quad \left. + \int_{I_{\text{HeII}}}^{\infty} \frac{L_E e^{-\tau(r,E)}}{E} \sigma_{\text{HeII}} \frac{n_{\text{HeII}}}{n_{\text{HI}}} N_{\text{s,HI}}(E - I_{\text{HeII}}) dE \right), \\ \Gamma_{\text{HeI}} &= \frac{1}{4\pi r^2} \left(\int_{I_{\text{HI}}}^{\infty} \frac{L_E e^{-\tau(r,E)}}{E} \sigma_{\text{HI}} \frac{n_{\text{HI}}}{n_{\text{HeI}}} N_{\text{s,HeI}}(E - I_{\text{HI}}) dE \right. \\ &\quad + \int_{I_{\text{HeI}}}^{\infty} \frac{L_E e^{-\tau(r,E)}}{E} \sigma_{\text{HeI}} (1 + N_{\text{s,HeI}}(E - I_{\text{HeI}})) dE \\ &\quad \left. + \int_{I_{\text{HeII}}}^{\infty} \frac{L_E e^{-\tau(r,E)}}{E} \sigma_{\text{HeII}} \frac{n_{\text{HeII}}}{n_{\text{HeI}}} N_{\text{s,HeI}}(E - I_{\text{HeII}}) dE \right), \\ \Gamma_{\text{HeII}} &= \frac{1}{4\pi r^2} \int_{I_{\text{HeII}}}^{\infty} \frac{L_E e^{-\tau(r,E)}}{E} \sigma_{\text{HeII}} dE, \end{aligned} \quad (12)$$

where $I_{\text{HI}} = 13.6$ eV, $I_{\text{HeI}} = 24.6$ eV and $I_{\text{HeII}} = 54.4$ eV are the ionization thresholds for HI, HeI and HeII, $N_{\text{s,HI}}$ and $N_{\text{s,HeI}}$ are the mean numbers of secondary ionizations of HI and HeI (secondary ionization of HeII is practically unimportant) caused by the fast photoelectron (their dependencies on energy are adopted from Furlanetto & Stoever 2010), and

$$\tau(r, E) = \int_0^r [n_{\text{HI}}(r')\sigma_{\text{HI}}(E) + n_{\text{HeI}}(r')\sigma_{\text{HeI}}(E) + n_{\text{HeII}}(r')\sigma_{\text{HeII}}(E)] dr' \quad (13)$$

is the IGM photoionization optical depth within radius r from the source, with the cross-sections $\sigma_{\text{HI}}(E)$, $\sigma_{\text{HeI}}(E)$ and $\sigma_{\text{HeII}}(E)$ adopted from Verner et al. (1996).

The evolution of the gas temperature with time in a given shell is given by

$$\frac{dT_K}{dt} = -2HT_K + \frac{T_K}{\mu} \frac{d\mu}{dt} + \frac{2\mu m_p}{3k\rho_b} (\mathcal{H} - \Lambda), \quad (14)$$

where the photoionization heating rate is given by

$$\begin{aligned} \mathcal{H} &= \frac{1}{4\pi r^2} \left(\int_{I_{\text{HI}}}^{\infty} \frac{L_E e^{-\tau(r,E)}}{E} (E - I_{\text{HI}}) n_{\text{HI}} \sigma_{\text{HI}} f_{\text{heat}}(E - I_{\text{HI}}) dE \right. \\ &\quad + \int_{I_{\text{HeI}}}^{\infty} \frac{L_E e^{-\tau(r,E)}}{E} (E - I_{\text{HeI}}) n_{\text{HeI}} \sigma_{\text{HeI}} f_{\text{heat}}(E - I_{\text{HeI}}) dE \\ &\quad \left. + \int_{I_{\text{HeII}}}^{\infty} \frac{L_E e^{-\tau(r,E)}}{E} (E - I_{\text{HeII}}) n_{\text{HeII}} \sigma_{\text{HeII}} f_{\text{heat}}(E - I_{\text{HeII}}) dE \right), \end{aligned} \quad (15)$$

with $H(z)$ being the Hubble constant, ρ_b the average baryonic density of the Universe, μ the mean molecular weight and f_{heat} the fraction of the photoelectron energy that goes into gas heating (Furlanetto & Stoever 2010).

The term proportional to Λ in equation (14) accounts for the radiative losses arising from collisional and recombinations processes (the corresponding rates were adopted

from Theuns et al. 1998), as well as for Compton cooling caused by scattering of the CMB on free electrons⁵), which proceeds on a time scale

$$t_{\text{CMB}} = \frac{3m_e c^2 (n/n_e)}{32\sigma_T \sigma T_{\text{CMB}}^4(z)} \approx 8 \times 10^7 \left(\frac{n_e}{n}\right)^{-1} \left(\frac{1+z}{11}\right)^{-4} \text{ yr.} \quad (16)$$

where n is the total particle number density, σ_T is the Thomson scattering cross-section and σ is the Stefan–Boltzmann constant, cooling due to collisional processes (including bremsstrahlung) and CMB scattering proves to be important in the vicinity of the miniquasar where the gas becomes strongly ionized and its temperature rises to $T_K \gtrsim 10^4$ K. However, the cooling processes typically have a negligible effect on the average parameters of the IGM heating zone produced by the miniquasar.

We further assume that the spin temperature, T_s , characterizing the 21 cm transition is everywhere equal to the gas kinetic temperature, T_K . The EDGES measurement (Bowman et al. 2018) suggests that it is indeed the case at $z \lesssim 20$, implying that by that time the first stars had already created a significant UV (10.2–13.6 eV) background for decoupling the spin temperature from the CMB temperature and bringing it close to the gas kinetic temperature via the Wouthuysen–Field effect (Wouthuysen 1952; Field 1958). Furthermore, photoionization of the IGM by soft X-rays from a miniquasar will be accompanied by the creation of Ly α photons that will further strengthen the Wouthuysen–Field effect wherever the gas temperature increases by $\gtrsim 10^3 H(z)t_S \gtrsim 100$ K on the BH growth timescale (Chuzhoy, Alvarez, & Shapiro 2006; Chen & Miralda-Escudé 2008). Under these assumptions and for the adopted cosmological parameters, the brightness temperature of the 21 cm line is expected to be

$$T_b = 29 x_{\text{HI}} \left(\frac{1+z}{11}\right)^{1/2} \left(1 - \frac{1+z}{11} \frac{30}{T_K}\right) \text{ mK.} \quad (17)$$

5 RESULTS

Our model has the following parameters: the initial and final redshifts (z_i and z_f), the initial and final masses of the BH (m_i and m_f , in solar masses), the Eddington ratio during active accretion phases (\dot{m}), and the intragalactic absorption column density and metallicity (N_{H} and Z , respectively). We now present a summary of results obtained for various sets of the parameter values.

5.1 Gas temperature and 21 cm brightness temperature radial profiles

Figure 3 shows the IGM temperature and hydrogen ionization fraction as functions of comoving distance from the miniquasar as well as the brightness temperature of the resulting 21 cm signal as a function of the angular distance in the plane of the sky for $z_i = 15$, $z_f = 10$, $m_i = 2 \times 10^3$, $m_f = 10^4$,

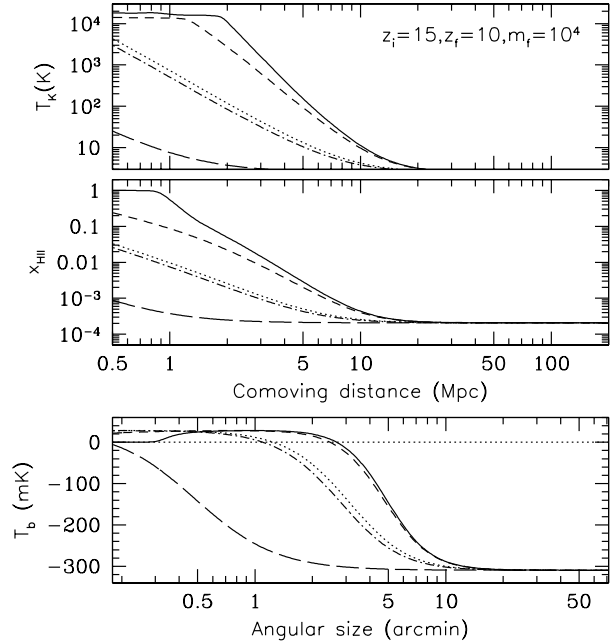


Figure 3. *Top panel:* IGM temperature as a function of comoving distance from the miniquasar for $z_i = 15$, $z_f = 10$, $m_i = 2 \times 10^3$, $m_f = 10^4$, $\dot{m} = 1$ and various parameters of intragalactic absorption [N_{H} (cm^{-2}), Z]: (10^{18} , 0) – solid line, (10^{20} , 0) – short-dashed line, (10^{21} , 0) – dotted line, (10^{22} , 0) – long-dashed line and (10^{21} , 1) – dash-dotted line. *Middle panel:* hydrogen ionization fraction. *Bottom panel:* 21 cm brightness temperature as a function of angular distance. These plots correspond to z_f .

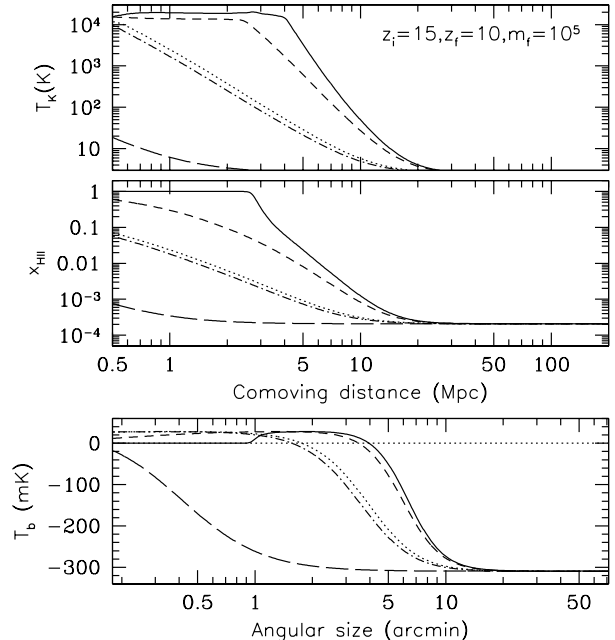


Figure 4. Same as Fig. 3, but for $m_i = 2 \times 10^4$ and $m_f = 10^5$.

⁵ Inverse Compton heating due to the X-ray radiation is negligible except very close to the miniquasar.

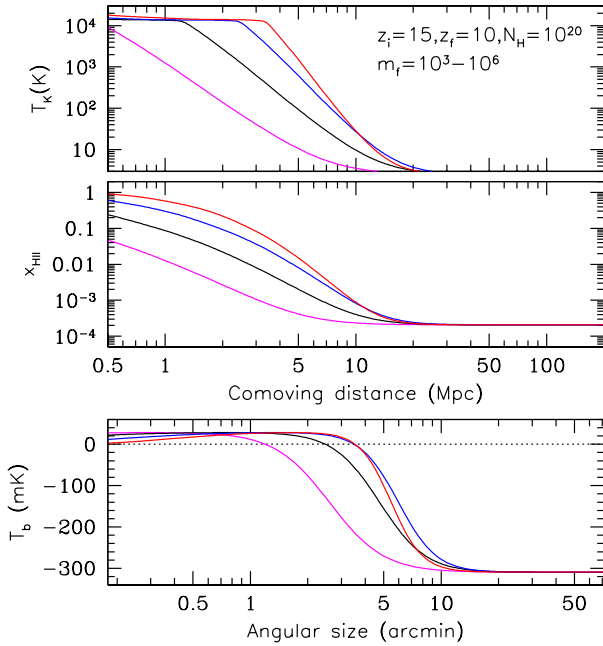


Figure 5. Similar to Fig. 3, but for a fixed absorption column ($N_{\text{H}} = 10^{20} \text{ cm}^{-2}$) and various BH masses (m_i, m_f): ($2 \times 10^2, 10^3$) – magenta, ($2 \times 10^3, 10^4$) – black, ($2 \times 10^4, 10^5$) – blue, ($2 \times 10^5, 10^6$) – red.

$\dot{m} = 1$ (the corresponding accretion duty cycle $k_{\text{duty}} = 40\%$) and various absorption characteristics: $Z = 0, N_{\text{H}} = 10^{18}, 10^{20}, 10^{21}, 10^{22} \text{ cm}^{-2}$ and $Z = 1, N_{\text{H}} = 10^{21}$. We see that absorption of soft X-rays within the host galaxy leads to less efficient IGM heating if $N_{\text{H}} \geq 10^{20} \text{ cm}^{-2}$ and that the presence of heavy elements ($Z = 1$ vs. $Z = 0$) proves to be of minor importance. Therefore, we hereafter focus on the metal-free case, unless specifically noted otherwise.

Figure 4 is analogous to Fig. 3, but the BH mass has been increased by an order of magnitude, from $m_i = 2 \times 10^3, m_f = 10^4$ to $m_i = 2 \times 10^4, m_f = 10^5$. We see that the influence of intragalactic absorption is similar to the previous case and that the IGM heating zone has somewhat spread outwards.

Figure 5 demonstrates the dependence of the results on the BH mass. Here, we adopted $z_i = 15, z_f = 10, \dot{m} = 1$ and $N_{\text{H}} = 10^{20}$ and sampled BH masses (m_i, m_f) from ($2 \times 10^2, 10^3$) to ($2 \times 10^6, 10^6$). We see that although more massive BHs produce much stronger ionization very close to the source, this has a fairly small effect on the resulting 21 cm signal, because the innermost region of strong heating is characterized by a nearly saturated, positive 21 cm brightness temperature [because $T_{\text{K}} \gg T_{\text{CMB}}$, see eq. (17)]. More important from an observational point of view is what happens at larger distances, where the 21 cm signal changes from emission to absorption, and we see that the effective size of this region first noticeably increases on going from $m_f = 10^3$ to $m_f = 10^4$ and then remains nearly the same for $m_f = 10^5$ and $m_f \leq 10^6$. This behavior is broadly consistent with the prediction made in §3 that the 21 cm zones around miniquasars should be largely determined by the total accretion energy for BHs with $M \lesssim 10^4 M_{\odot}$ and by the characteristic mean free path of accretion disk photons for more massive BHs.

Figure 6 demonstrates the influence of a particular his-

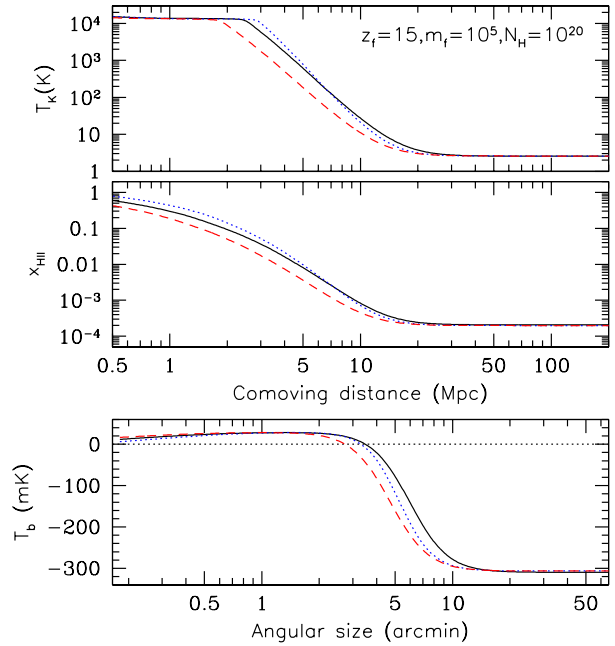


Figure 6. Similar to Fig. 3, but for fixed BH masses ($m_i = 2 \times 10^4, m_f = 10^5$) and absorption column ($N_{\text{H}} = 10^{20} \text{ cm}^{-2}$) and various scenarios of BH growth (z_i, z_f, \dot{m}): (15, 10, 1) – black solid line, (20, 10, 1) – blue dotted line, (20, 10, 0.5) – red dashed line.

tory of BH growth on the results. Here, we fixed the final redshift at $z_f = 10$, the initial and final BH masses at $m_i = 2 \times 10^4$ and 10^5 , respectively, and the absorption column at $N_{\text{H}} = 10^{20}$, and considered three scenarios: (i) $z_i = 15, \dot{m} = 1$ (the duty cycle $k_{\text{duty}} = 40\%$), (ii) $z_i = 20, \dot{m} = 1$ ($k_{\text{duty}} = 27\%$) and (iii) $z_i = 20, \dot{m} = 0.5$ ($k_{\text{duty}} = 55\%$). We see that the differences in the corresponding T_{K} and T_{b} profiles are small.

So far we have assumed that the incident radiation spectrum is that of a multicolor accretion disk modified by line-of-sight absorption, as shown in Fig. 1. We now wish to investigate the possible effect of an additional hard, powerlaw spectral component that may arise due to Comptonization in a hot corona of the BH accretion disk. To this end, we carried out calculations for our *simpl*diskbb* spectral models for $m_f = 10^4, 10^5$ and 10^6 and $N_{\text{H}} = 10^{20} \text{ cm}^{-2}$, shown in Fig. 2. The resulting $T_{\text{K}}, x_{\text{HII}}$ and T_{b} radial profiles are compared in Fig. 7 with those computed without a hard X-ray component. We see that the 21 cm zone is almost unaffected by the hard spectral component for the least massive BH ($m_f = 10^4$), somewhat broadens in the intermediate mass case ($m = 10^5$), and becomes substantially (by a factor of ~ 2) broader for the heaviest BH ($m = 10^6$). The last result is unsurprising, because the corresponding X-ray spectrum (see Fig. 2) is dominated by the powerlaw component already at $E \sim 300 \text{ eV}$ (partially because of the adopted substantial line-of-sight absorption of 10^{20} cm^{-2}).

5.2 Characteristic size of the 21 cm zone

From the above comparison of the computed T_{b} radial profiles, a preliminary conclusion may be drawn that the spatial extent of the 21 cm signal associated with a high-redshift

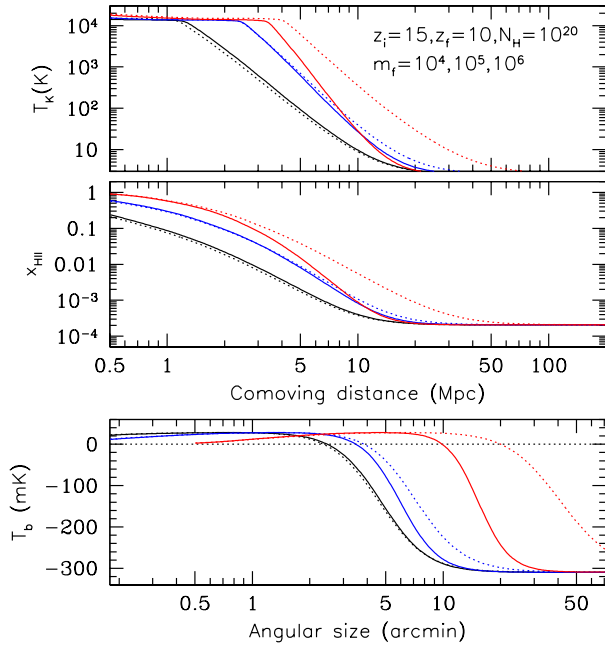


Figure 7. Similar to Fig. 3, for a fixed absorption column ($N_{\text{H}} = 10^{20} \text{ cm}^{-2}$, $Z = 0$), three sets of BH masses ($m_i = 2 \times 10^3$, $m_f = 10^4$ – black, $m_i = 2 \times 10^4$, $m_f = 10^5$ – blue, $m_i = 2 \times 10^5$, $m_f = 10^6$ – red) and two spectral models: pure thermal disk emission (*diskbb* – solid) and thermal disk emission with a Comptonization tail (*simpl*diskbb* – dotted).

miniquasar is expected to depend only weakly on the properties of the latter. For more quantitative assessment, we define two characteristic angular sizes: θ_0 – the projected distance from the miniquasar at which the 21 cm signal changes from emission to absorption, i.e. $T_{\text{b}} = 0$, and $\theta_{1/2}$ – the radius at which the brightness temperature of the absorption signal is half the ‘background’ value (the 21 cm brightness temperature outside of the miniquasar heating zone), i.e. $T_{\text{b}} = T_{\text{b,bgr}}/2$. Under our assumptions that there is no global IGM heating and that the 21 cm spin temperature is coupled to the IGM kinetic temperature, $T_{\text{b,bgr}} = -245 \text{ mK}$ and -307 mK at $z_i = 15$ and $z_f = 10$, respectively.

Figure 8 shows θ_0 and $\theta_{1/2}$ as functions of the absorption column for $z_i = 15$, $z_f = 10$, $\dot{m} = 1$ and three different BH masses, $m_f = 10^4$, 10^5 and 10^6 . We see that if the intragalactic absorption is not strong ($N_{\text{H}} \lesssim 10^{20} \text{ cm}^{-2}$), both θ_0 and $\theta_{1/2}$ depend very weakly on the BH mass. Specifically, $\theta_0 \sim 3\text{--}4 \text{ arcmin}$, and $\theta_{1/2} \sim 5\text{--}6 \text{ arcmin}$. If $N_{\text{H}} \gtrsim 10^{21} \text{ cm}^{-2}$, most of the microquasar’s soft X-ray emission is absorbed within its host galaxy, which naturally leads to a dramatic weakening of IGM heating and shrinkage of the 21 cm zone. Figure 9 shows a similar set of curves for the case of miniquasars operating at higher redshifts, namely $z_i = 20$ and $z_f = 15$. In this case, there is a more noticeable, albeit still weak dependence on the BH mass, namely (for $N_{\text{H}} \lesssim 10^{20} \text{ cm}^{-2}$) θ_0 changes from ~ 1.5 to $\sim 3 \text{ arcmin}$ as m_f increases from 10^4 to 10^6 , whereas $\theta_{1/2}$ changes from ~ 2.5 to $\sim 4.5 \text{ arcmin}$ in the same BH mass range. Overall, the computed θ_0 size of the heating zone is in remarkably good agreement (within a factor of ~ 2) with our rough prediction given by equation (8).

The next two figures, Fig. 10 and Fig. 11, demonstrate

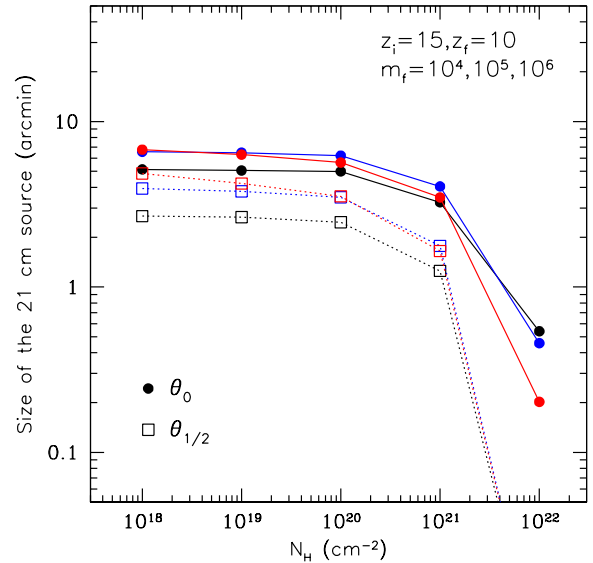


Figure 8. Characteristic angular sizes (see text for definitions) θ_0 (empty squares connected by dotted lines) and $\theta_{1/2}$ (filled circles connected by solid lines) of the 21 cm signal around a miniquasar as a function of the absorption column for $z_i = 15$, $z_f = 10$, $\dot{m} = 1$ and three different sets of BH masses (m_i, m_f): ($2 \times 10^3, 10^4$) – black, ($2 \times 10^4, 10^5$) – blue, and ($2 \times 10^5, 10^6$) – red.

the impact of an additional hard (Comptonization) spectral component on the extent of the miniquasar 21 cm zone. By comparing these plots with those pertaining to the case of pure multicolor disk emission (Fig. 8 and Fig. 9, respectively), we see that while θ_0 and $\theta_{1/2}$ have remained nearly unchanged for $m_f \leq 10^5$, the characteristic radii have increased substantially (by a factor of $\sim 1.5\text{--}2$) for $m_f = 10^6$. Therefore, the hard tail considerably changes the overall picture for the most massive (within the considered range) BHs ($m = 10^6$). This reflects the fact that, within the adopted model, the Comptonized radiation starts to dominate over the thermal emission already at photon energies $\sim 300 \text{ eV}$.

5.3 Spectrum and flux of the 21 cm signal

We now discuss the spectral properties of the 21 cm signal that could be measured from the vicinity (both in space and redshift) of miniquasars by future radio telescopes. As is clear from the above results, the position of a miniquasar on the sky will be surrounded by a well-defined region with a size of several arcmin within which $T_{\text{b}} - T_{\text{b,bgr}} \gtrsim 100 \text{ mK}$. One could then try to search for an excess 21 cm emission from this region.

In reality, the optimal size of the signal extraction region should be chosen taking into account the characteristics of a particular radio telescope, but it is clear that it should be of the order of the $\theta_{1/2}$ radius defined above. We therefore integrated the surface brightness of the expected 21 cm excess emission (i.e. the difference $T_{\text{b}} - T_{\text{b,bgr}}$) over the circle of radius $\theta_{1/2}$ around the miniquasar.

Figure 12 shows the resulting spectra for $z_i = 15$, $z_f = 10$,

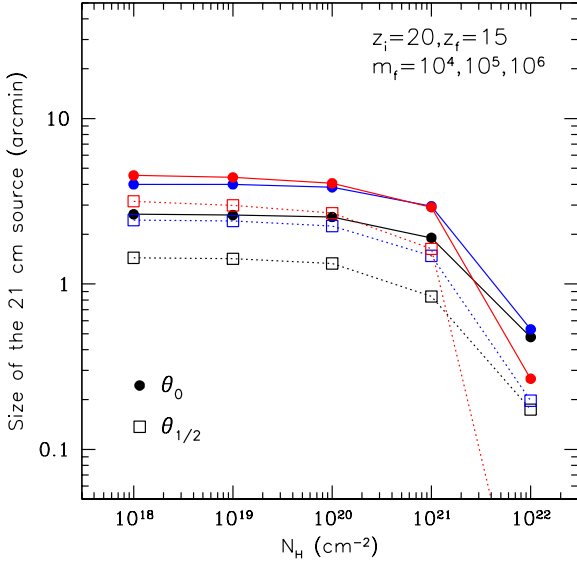


Figure 9. Same as Fig. 8, but for $z_i = 20$ and $z_f = 15$.

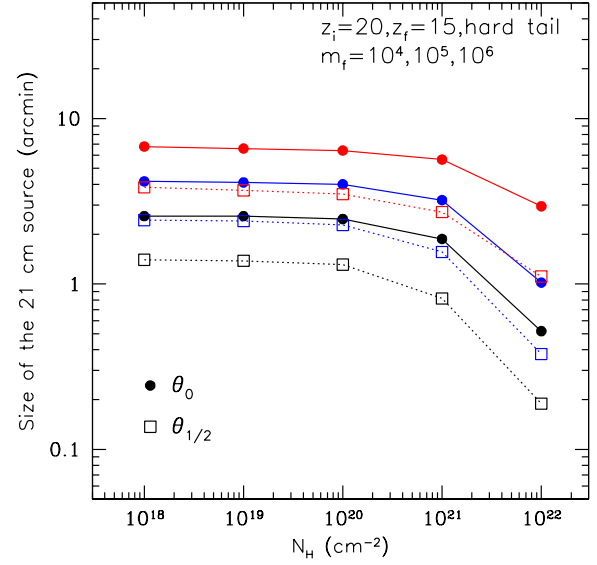


Figure 11. Same as Fig. 9, but for thermal disk emission with a Comptonization tail (*simpl*diskbb*) instead of pure thermal disk emission.

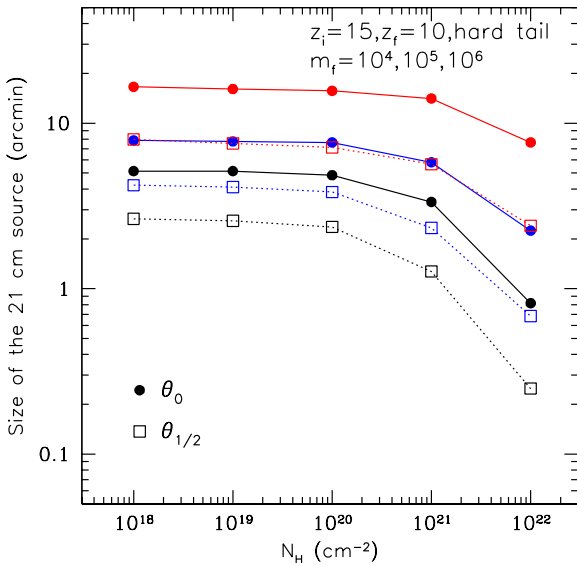


Figure 10. Same as Fig. 8, but for thermal disk emission with a Comptonization tail (*simpl*diskbb*) instead of pure thermal disk emission.

$m_i = 2 \times 10^4$, $m_f = 10^5$, $\dot{m} = 1$ and various absorption columns. We see that the 21 cm flux density is almost unaffected by intragalactic absorption if $N_H \lesssim 10^{20} \text{ cm}^{-2}$, the signal weakens by a factor of ~ 3 for $N_H = 10^{21} \text{ cm}^{-2}$ and practically vanishes if $N_H = 10^{22} \text{ cm}^{-2}$, as essentially no soft X-rays from the miniquasar leak from the host galaxy into the IGM.

Figure 13 demonstrates the dependence of the 21 cm spectrum on the BH mass (for $z_i = 15$, $z_f = 10$, $\dot{m} = 1$ and

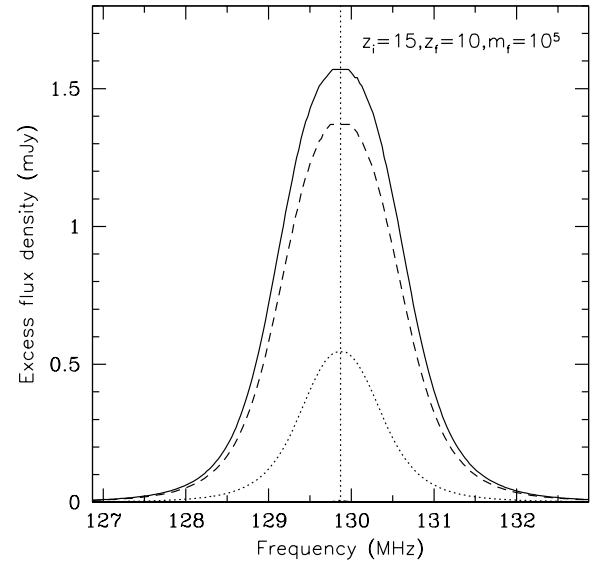


Figure 12. Spectra of 21 cm excess emission (with respect to the background level at the miniquasar's redshift) integrated within $\theta_{1/2}$ for $z_i = 15$, $z_f = 10$, $\dot{m} = 1$, $m_i = 2 \times 10^4$, $m_f = 10^5$ and various N_H columns (cm^{-2}): 10^{18} – solid line, 10^{20} – dashed line, 10^{21} – dotted line, 10^{22} – dash-dotted line (poorly visible near the lower boundary of the plot).

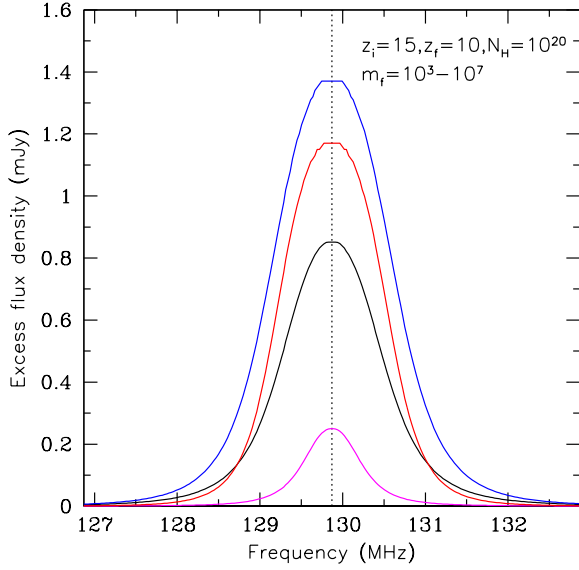


Figure 13. Similar to Fig. 12, but for a fixed absorption column ($N_{\text{H}} = 10^{20} \text{ cm}^{-2}$) and various BH masses (m_i, m_f): ($2 \times 10^2, 10^3$) – magenta, ($2 \times 10^3, 10^4$) – black, ($2 \times 10^4, 10^5$) – blue, ($2 \times 10^5, 10^6$) – red.

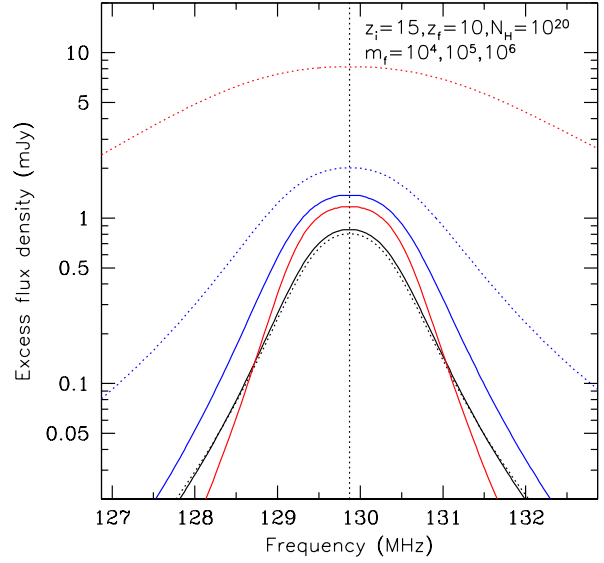


Figure 15. Similar to Fig. 13, comparing the case of pure thermal disk emission (*diskbb*, solid curves) with that of disk emission and a Comptonization tail (*simpl*diskbb*, dotted curves), for three sets of BH masses (m_i, m_f): ($2 \times 10^3, 10^4$) – black, ($2 \times 10^4, 10^5$) – blue and ($2 \times 10^5, 10^6$) – red. Note the logarithmic vertical scale.

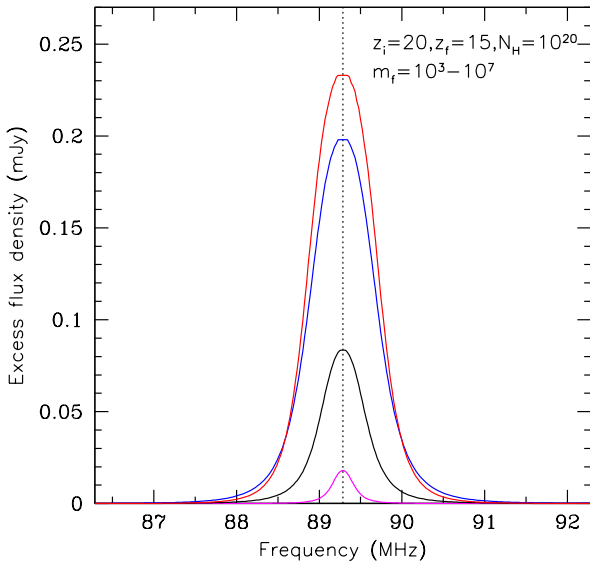


Figure 14. Same as Fig. 13, but for higher redshifts, $z_i = 20$, $z_f = 15$.

$N_{\text{H}} = 10^{20} \text{ cm}^{-2}$). We see that the signal increases by a factor of ~ 3 on going from $m_f = 10^3$ to 10^4 , by another factor of ~ 1.5 on going to $m_f = 10^5$ and then remains nearly the same for $m_f = 10^6$. Figure 14 shows the corresponding spectra for similar miniquasars at higher redshifts, $z_i = 20$, $z_f = 15$. The picture is qualitatively similar to the previous case. Most

importantly, Figs. 13 and 14 demonstrate that the expected 21 cm signal depends very weakly on the BH mass.

Figures 15 and 16 demonstrate the impact of an additional hard spectral component on the discussed 21 cm spectra. We see that the hard tail leads to a dramatic increase of the expected 21 cm signal for our most massive ($m_f = 10^6$) BH, with the difference being more pronounced for the lower redshift case ($z_f = 10$ vs. $z_f = 15$). These tendencies are expected, since the reported spectra were obtained by integration of T_{b} within the characteristic radius $\theta_{1/2}$, which increases in the presence of a hard spectral component, as was shown in §5.2.

As regards the absolute value of the expected 21 cm flux density, it is useful to approximate it as follows:

$$F_{\nu} \approx \frac{2k}{(21 \text{ cm})^2(1+z)^2} \frac{3|T_{\text{b,bgr}}|}{4} \pi \theta_{1/2}^2, \\ \approx 0.6 \left(\frac{1+z_f}{11} \right)^{-2} \frac{|T_{\text{b,bgr}}|}{250 \text{ mK}} \left(\frac{\theta_{1/2}}{5'} \right)^2 \text{ mJy}, \quad (18)$$

where we assumed that the average excess brightness temperature of the 21 cm signal within $\theta_{1/2}$ is $3T_{\text{b,bgr}}/4$, which is approximately the case (see the T_{b} radial profiles in §5.1). Substituting the typical values derived from our simulations for $z_f = 10$ ($T_{\text{b,bgr}} = -309 \text{ mK}$, $\theta_{1/2} = 6'$) and $z_f = 15$ ($T_{\text{b,bgr}} = -245 \text{ mK}$, $\theta_{1/2} = 4'$) into the above expression, we find $F_{\nu} \approx 1.1$ and 0.18 mJy , respectively, in good agreement with the 21 cm spectra shown above.

We finally note that the simulated 21 cm spectra for the case of purely thermal disk emission are all characterized by nearly the same FWHM of ≈ 0.01 in terms of $\Delta\nu/\nu$.

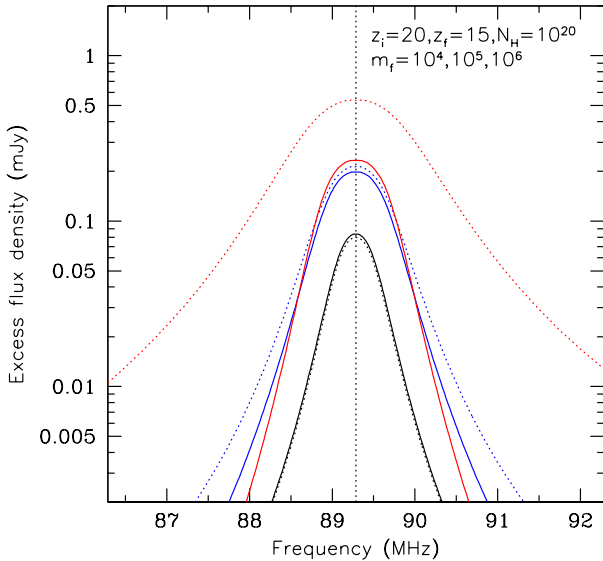


Figure 16. Similar to Fig. 15, but for higher redshifts, $z_i = 20$, $z_f = 15$.

6 RELATION TO X-RAY OBSERVATIONS

As was discussed in §1, there is a hope that future X-ray observatories such as *Lynx* will be able to find a significant number of high-redshift miniquasar candidates. Provided that the planned next-generation radio facilities such as *SKA* are also available by that time, it should be possible to search for the specific 21 cm signatures of X-ray selected miniquasars discussed in this study.

The first practical question is then: what are the limiting BH mass and redshift for X-ray detection of miniquasars? In this study, we have assumed that the miniquasar’s spectrum consists of (i) multicolor disk emission with a temperature expected from the standard accretion disk theory and, possibly, (ii) a hard, power-law ($\Gamma = 2$) tail, associated with Comptonization of disk emission in a hot corona, which extends to high energies (at least to tens of keV). It is this additional hard component that an X-ray telescope might be able to detect from a high-redshift miniquasar. In the particular spectral model, *simpl(diskbb)*, used in this study, the observed X-ray flux in the 0.5–2 keV band (corresponding to emission in a rest-frame band of $0.5(1+z)$ – $2(1+z)$ keV), F_X , is proportional to the fraction of scattered photons. It turns out that, virtually independently of the BH mass and accretion rate,

$$F_X \approx 0.06 \frac{f_{sc}}{0.05} \frac{L}{4\pi D_L^2}, \quad (19)$$

where L is the total luminosity of the miniquasar and $D_L(z)$ is the luminosity distance.

Assuming that $f_{sc} = 0.05$ (which is a reasonable value as discussed in §2.2) and that the X-ray telescope catches the miniquasar when it is accreting at a critical rate ($\dot{m} = 1$), i.e. that $L = L_{Edd}(m)$, we find from equation (19) that for $m = 10^4$, $F_X = 2.3 \times 10^{-20}$ and 5.8×10^{-20} erg cm $^{-2}$ s $^{-1}$ for $z = 15$ and $z = 10$, respectively, whereas for $m = 10^5$, $F_X = 2.3 \times 10^{-19}$

and 5.8×10^{-19} erg cm $^{-2}$ s $^{-1}$ for the same redshifts. These fluxes are well below the detection threshold of *Chandra* – the most sensitive existing X-ray telescope. However, *Lynx* is expected to reach a sensitivity of $\sim 10^{-19}$ erg cm $^{-2}$ s $^{-1}$ in its deep extragalactic surveys and should thus be able to detect actively growing BHs with mass $\gtrsim 5 \times 10^4 M_\odot$ at $z = 15$ and $\gtrsim 2 \times 10^4 M_\odot$ at $z = 10$. These mass limits are of course inversely proportional to \dot{m} and f_{sc} .

7 DISCUSSION AND SUMMARY

We have shown that an intermediate mass BH growing by radiatively efficient accretion in the early Universe should leave a specific, localized imprint on the 21 cm cosmological signal. Namely, a BH of mass between $\sim 10^4$ and $\sim 10^6 M_\odot$ at $z \sim 15$ – 10 is expected to be surrounded by a region with a fairly sharp boundary of several arcmin radius, within which the 21 cm temperature quickly grows inwards from the background value $T_{b,bgr} \sim -200$ mK to $T_b \sim 0$ (reaching the saturation value of ~ 30 mK in the innermost region). Most interestingly, the size of this region is almost insensitive to the BH mass in the range quoted above, so that the flux density of the excess 21 cm signal is expected to take a nearly universal value (with a trivial redshift dependence), approximately given by equation (18).

7.1 Sensitivity to assumptions

The above result was obtained under certain assumptions and it is important to discuss how realistic they are. Perhaps, the most important constituent of our model is the miniquasar’s energy spectrum, which we assumed to be that of multicolor disk blackbody emission. As was discussed in §2.1 the actual shape of the disk’s spectrum is likely to deviate significantly from that adopted in our treatment, but given the insensitivity of the size of the 21 cm zone to the BH mass, such deviations are unlikely to have a significant effect on the results. More important is the likely presence of an additional, hard component in the miniquasar spectrum. As we have demonstrated, its effect is small for relatively low-mass BHs ($\sim 10^4$ – $10^5 M_\odot$) but becomes substantial (the heating zone widens by a factor of ~ 1.5 – 2) for a $10^6 M_\odot$ BH.

The next important issue is that of possible photoabsorption of the miniquasar’s soft X-ray emission within its host galaxy. It turns out that the properties of the 21 cm zone remain nearly unchanged as long as $N_H \lesssim 10^{20}$ cm $^{-2}$ (regardless of the presence of metals in the absorbing medium), but starting at $N_H \sim 10^{21}$ cm $^{-2}$ this zone starts to shrink dramatically. One may argue that a powerful miniquasar should be able to quickly photoionize the interstellar medium within a substantial distance of itself and thus effectively reduce N_H (e.g. [Sazonov & Khabibullin 2018](#)), but this clearly needs further investigation. Furthermore, if miniquasars are less powerful analogs of AGN, they may have a small-scale obscuring torus of cold gas and dust. In that case there will be two opposite cones of specific 21 cm signal around the miniquasar, i.e. the average signal within the $\theta_{1/2}$ radius will decrease by a factor of $\Omega/4\pi$, where Ω is the solid angle of the unobscured sky as seen from the BH.

Finally, we assumed that the Universe had not yet been globally heated at the redshifts of interest ($z \sim 15$ – 10) and

that the 21 cm spin temperature was coupled to the gas temperature at these epochs. It is only in this case that a large contrast in the 21 cm brightness temperature arises between the vicinity of the miniquasar, where $T_b \sim 0$, and the background, where $T_b \sim -(200\text{--}300)$ mK (at $z = 15\text{--}10$). These assumed conditions are in good agreement with the recent EDGES result (Bowman et al. 2018) for $z \sim 20\text{--}15$ ⁶ but appear to fail at $z \lesssim 14$, when the global 21 cm temperature is measured to be around zero. Of course, the EDGES measurements must be verified with future observations but a lot of authors (see §1) have suggested that XRBs, miniquasars and other types of X-ray sources can indeed significantly heat the Universe by $z \sim 10$. In such a case, it will be extremely difficult to discern the 21 cm imprint of an individual miniquasar against the background at $z \sim 10$ but it should still be possible to do at $z \sim 15$.

7.2 Observational strategy

A blind sky search for weak 21 cm signals associated with individual high-redshift miniquasars might not be feasible in the near future. Therefore, we propose to look for such signals from miniquasar candidates that might be found with a next-generation X-ray mission such as *Lynx*. As discussed in §6 (see also Ben-Ami, Vikhlinin, & Loeb 2018), the planned sensitivity of *Lynx* of $\sim 10^{-19}$ erg cm⁻² s⁻¹ should allow it to detect rapidly growing BHs with a mass as low as a few $10^4 M_\odot$ out to $z \sim 15$, provided that a significant fraction of the energy released by accretion goes into Comptonized, hard X-ray radiation. Unfortunately, it should be very difficult to measure the redshifts of such extremely faint objects and their host galaxies even with the next-generation optical/IR telescopes such as *JWST* and ELT. However, it might be possible to identify such objects using future 21 cm observations with a next-generation radio telescope array such as SKA.

The low-frequency component of the latter, SKA-low, is planned to cover a broad frequency range extending down to ~ 50 MHz (allowing one to probe the early Universe out to $z \sim 25$) with high spectral resolution (~ 1 kHz) and a very large collecting area ~ 1 km². It is hoped that SKA will enable 21 cm tomography at a few mK level on a few arcmin scales (Mellema et al. 2013). According to our estimates, high-redshifts miniquasars are expected to produce 21 cm signals with an amplitude of ~ 100 mK on a few arcmin scale and should thus be detectable by SKA-low. Perhaps, an optimal strategy would be to compare the 21 cm signal accumulated within a few arcmin aperture around the X-ray position of a miniquasar candidate with the 21 cm background level by probing one redshift slice after another over a range of $z \sim 10\text{--}20$. The detection of a positive signal $\sim 0.5[(1+z)/11]^{-2}$ mJy [see eq. (18)] will strongly indicate that the object is an intermediate-mass BH growing to become a supermassive BH. Moreover, its redshift can thus be measured to within $\Delta z/(1+z) \lesssim 0.01$, since the FWHM of the expected 21 cm signal is about 1%.

⁶ Actually, EDGES measured an even lower sky-averaged $T_b \sim -500$ mK.

ACKNOWLEDGMENTS

The research was supported by the Russian Science Foundation (grant 14-12-01315).

REFERENCES

- Arnaud K. A., 1996, ASPC, 101, 17
 Bañados E., et al., 2018, Natur, 553, 473
 Ben-Ami S., Vikhlinin A., Loeb A., 2018, ApJ, 854, 4
 Bolgar F., Eames E., Hottier C., Semelin B., 2018, MNRAS, 478, 5564
 Bowman J. D., Rogers A. E. E., Monsalve R. A., Mozdzen T. J., Mahesh N., 2018, Natur, 555, 67
 Chen X., Miralda-Escudé J., 2008, ApJ, 684, 18
 Chuzhoy L., Alvarez M. A., Shapiro P. R., 2006, ApJ, 648, L1
 Cohen A., Fialkov A., Barkana R., Lotem M., 2017, MNRAS, 472, 1915
 Davis S. W., Blaes O. M., Hubeny I., Turner N. J., 2005, ApJ, 621, 372
 Done C., Gierliński M., Kubota A., 2007, A&ARv, 15, 1
 Done C., Davis S. W., Jin C., Blaes O., Ward M., 2012, MNRAS, 420, 1848
 Elvis M., et al., 1994, ApJS, 95, 1
 Ferrara A., Loeb A., 2013, MNRAS, 431, 2826
 Fialkov A., Cohen A., Barkana R., Silk J., 2017, MNRAS, 464, 3498
 Field G. B., 1958, PIRE, 46, 240
 Fragos T., et al., 2013, ApJ, 764, 41
 Furlanetto S. R., Stoever S. J., 2010, MNRAS, 404, 1869
 Ghara R., Choudhury T. R., Datta K. K., Choudhuri S., 2017, MNRAS, 464, 2234
 Gilfanov M., Merloni A., 2014, SSRv, 183, 121
 Koratkar A., Blaes O., 1999, PASP, 111, 1
 Latif M. A., Ferrara A., 2016, PASA, 33, e051
 Leite N., Evoli C., D’Angelo M., Ciardi B., Sigl G., Ferrara A., 2017, MNRAS, 469, 416
 Madau P., Rees M. J., Volonteri M., Haardt F., Oh S. P., 2004, ApJ, 604, 484
 Madau P., Fragos T., 2017, ApJ, 840, 39
 Makishima K., Maejima Y., Mitsuda K., Bradt H. V., Remillard R. A., Tuohy I. R., Hoshi R., Nakagawa M., 1986, ApJ, 308, 635
 Mellema G., et al., 2013, ExA, 36, 235
 Merloni A., Fabian A. C., Ross R. R., 2000, MNRAS, 313, 193
 Mirabel I. F., Dijkstra M., Laurent P., Loeb A., Pritchard J. R., 2011, A&A, 528, A149
 Pritchard J. R., Furlanetto S. R., 2007, MNRAS, 376, 1680
 Pritchard J. R., Loeb A., 2012, RPPH, 75, 086901
 Ricotti M., Ostriker J. P., 2004, MNRAS, 352, 547
 Ross H. E., Dixon K. L., Iliev I. T., Mellema G., 2017, MNRAS, 468, 3785
 Sazonov S. Y., Ostriker J. P., Sunyaev R. A., 2004, MNRAS, 347, 144
 Sazonov S., Sunyaev R., 2015, MNRAS, 454, 3464
 Sazonov S., Khabibullin I., 2017, Astron. Lett., 43, 243
 Sazonov S., Khabibullin I., 2018, MNRAS, 476, 2530
 Sazonov S. Y., Lutovinov A. A., Krivonos R. A., 2014, AstL, 40, 65
 Seager S., Sasselov D. D., Scott D., 1999, ApJ, 523, L1
 Shakura N. I., Sunyaev R. A., 1973, A&A, 24, 337
 Steiner J. F., Narayan R., McClintock J. E., Ebisawa K., 2009, PASP, 121, 1279
 Telfer R. C., Zheng W., Kriss G. A., Davidsen A. F., 2002, ApJ, 565, 773
 Theuns T., Leonard A., Efsthathiou G., Pearce F. R., Thomas P. A., 1998, MNRAS, 301, 478

Thomas R. M., Zaroubi S., 2008, MNRAS, 384, 1080
Vasiliev E. O., Sethi S. K., Shchekinov Y. A., 2018, ApJ, 865, 130
Verner D. A., Ferland G. J., Korista K. T., Yakovlev D. G., 1996,
ApJ, 465, 487
Volonteri M., 2010, A&ARv, 18, 279
Woods T. E., et al., 2018, arXiv, arXiv:1810.12310
Wouthuysen S. A., 1952, AJ, 57, 31

This paper has been typeset from a $\text{\TeX}/\text{\LaTeX}$ file prepared by the author.